Effect of in content on thermoelectric performance of InxGa1−xN alloys: Hybrid density functional theory study based on realistic models

Effect of In content on thermoelectric performance of $In_xGa_{1-x}N$ alloys: Hybrid density functional theory study based on realistic models

H.C. Aroussi[a,b], N.L. Marana[c,b], F. Hamdache[a], R. Houaria[a,d], S. Bahlouli[a], S. Casassa[b,*]

[a] *Laboratoire LPPMCA, Départment de Physique, Université des Sciences et de la Technologie Mohamed Boudiaf, Oran, Algeria*
[b] *Theoretical Chemistry Group, Dipartimento di Chimica, Università di Torino, Italy*
[c] *Modeling and Molecular Simulation Group, São Paulo State University, Bauru, Brazil*
[d] *University Mustapha Stambouli de Mascara, Mascara, Algeria*

Abstract

In this study, first-principles periodic calculations with localized Gaussian type orbitals within a hybrid density functional theory approach were performed to study the electronic, structural, thermodynamic, and transport properties of $In_xGa_{1-x}N$ nitride alloys. The compositions were modeled in the range of $0.06 < x < 0.87$ using a 32-atom supercell. According to previous studies, significant composition-dependent gap bowing occurs for both the lattice parameters and energy band gap. Our study of the thermodynamic stability indicated a notable trend toward spinodal decomposition. Infrared spectra are used as fingerprints to uniquely determine the composition and structure of alloys. Based on the transport properties calculated in the present study (Seebeck coefficient, power factor, and figure of merit), the ternary structure with $\approx 20\%$ In is the optimal thermoelectric material and preliminary investigations confirmed that the transport properties can be altered by point defects.

Key words: Nitride ternary alloys, hybrid functional, thermoelectrics, thermodynamics, defects

*silvia.casassa@unito.it

1. Introduction

In recent years, semiconductor materials have emerged as among the most important research topics because their promising properties can be exploited in several different application areas[1]. In particular, the growing demand for energy has increased the need for efficient devices and much research has focused on optoelectronic and photovoltaic materials [2]. Among the most widely studied materials, the compounds obtained as alloys of group 13–15 members are highly important, particularly gallium nitride (GaN) and indium nitride (InN), which share a wurtzite-like hexagonal structure and have band gaps of 3.40 eV and 0.77 eV, respectively.

$In_xGa_{1-x}N$ ternary alloys are attracting both scientific and technological interest because of the following reasons. $In_xGa_{1-x}N$ compounds are hard semiconductors with the ability to withstand high doses of radiation while also maintaining their optoelectronic properties[3, 4, 5]. Hence, by varying the In composition, the band gap can cover the entire electromagnetic spectrum from the visible to ultraviolet regions, making these ternaries suitable for use in various optoelectronic devices such as laser diodes and light-emitting diodes[6, 7, 8].
Moreover, these alloys exhibit strong optical absorption, $10^4 - 10^5$ cm^{-1}, which changes according to the percentage of indium, and thus they are adequate chemical sensors with a high saturation rate[9, 10, 11]. In addition to the aforementioned properties, $In_xGa_{1-x}N$ possess interesting thermoelectric characteristics because the percentage of indium tunes the direct band gap but also affects the thermal conductivity[12]. In particular, these materials are among the most promising thermoelectrics for use at room temperature, with figures of merit between 0.07[13]-0.08[14] for $0.2 < x < 0.36$. In/GaN have further advantages given the possibility of their simple integration with common nitride devices as well as their hardness and resistance to radiation, and nontoxic nature. The widespread production of III-nitride for light-emitting diodes and electronic devices can also drastically reduce their manufacturing cost.

Many theoretical studies[15, 16, 17, 18, 19] have explored these materials from different perspectives in order to explain and rationalize experimentally observed phenomena.

However, to the best of our knowledge, the present study is the first periodic *ab initio* investigation to be performed at the B3LYP level by using

localized atomic orbitals to expand the crystalline Bloch functions as well as investigating the modifications of several fundamental properties of the materials induced by increasing the indium concentration. The remainder of this paper is organized as follows. In the next section, the computational methods and models are presented and described. The *Results and Discussion* Section is subdivided into *subsections* that describe the structural (lattice parameters, bulk modulus and its first-order pressure derivative B) electronic (band gap, band structures, and density of states), thermodynamic, vibrational, and thermoelectric (S, PF, σ, and ZT) properties of the ternary $In_xGa_{1-x}N$ alloys over the range of $0 < x < 1$. Results and general trends are discussed relative to previously reported experimental and computational data where available.

We aim to provide a complete description of In/Ga nitride alloys and preliminary study on the role of point defects and atomic configurations in the emergence of new features. In order to facilitate the experimental design of these materials, some structure–property relationships are suggested and a consistent background is proposed for further computational modeling.

2. Computational details

2.1. Computational Method

Periodic simulations were performed using the global hybrid density functional B3LYP[20, 21] with 17% of "exact-exchange", as implemented in the CRYSTAL package[22], which we refer to as B3LYP-17 in the following (the exact formulation is provided in the Supplementary Information). The introduction of an appropriate amount of exact exchange is known to improve the accuracy of properties that depend on the extent of electronic delocalization, i.e., band gaps, phonon spectra, and transport parameters [23]. The density functional theory (DFT) exchange-correlation contribution was evaluated by numerical integration over the unit cell volume using a pruned grid with 99 radial and 1454 angular points. Integration over the reciprocal space was conducted using a Monkhorst–Pack mesh comprising 24 **k**-points in the first Brillouin zone.

Gallium, indium, and nitrogen were described by all-electron bases identified as Pandey94[24], Weihrich14[25], and Roetti90[26], respectively, which have been successfully tested on similar compounds in previous studies[27, 28].

The Coulomb and exchange series summed in direct space were truncated using overlap criteria thresholds of [8,8,8,8,16]. Convergence for the self-consistent field algorithm was achieved up to a threshold of 10^{-9} hartrees on the total energy per unit cell [29].
Geometry optimization was performed using analytical gradients with respect to the atomic coordinates and unit-cell parameters within a quasi-Newtonian scheme combined with Broyden–Fletcher–Goldfarb–Shanno Hessian updating [30, 31]. The default convergence criteria were employed for both the gradient components and nuclear displacements. The bulk modulus, B, and its first-order pressure derivative, B', were calculated with Murnaghan's equation of state[32, 33].

The full set of vibrational frequencies in Γ was obtained within the harmonic approximation by diagonalizing the mass-weighted Hessian matrix. This matrix was built by numerically differencing the analytical gradient with respect to atomic Cartesian coordinates. The zero-point energy (ZPE) and thermal contributions to the vibrational energy (E_{vib}) and entropy (S_{vib}) were calculated by considering the eigenvalues in Γ, and then added to the self-consistent field energy and pressure *per* volume term (P·V) to obtain the Gibbs free energy at room temperature. It should be noted that the supercell approach allows a few vibrational modes to be calculated with frequencies projected in Γ, but the thermodynamic analysis could be improved further by including larger phonon sampling.

The infrared (IR) intensities of the normal modes in Γ were evaluated with the Berry phase approach[34] and the absorption spectra were produced using Lorentzian broadening.

The Seebeck coefficient (S), electrical conductivity (σ), power factor (PF), and electron contribution to the thermal conductivity (κ_e) were computed using the semi-classical Boltzmann transport equation theory[35] and the frozen band approximation, where it was assumed that the energy relaxation time for carriers, τ, is a constant parameter that depends only on the indium composition[36]. In particular, we used $\tau = 10$ fs for GaN, where this value is in the range of Stanton observations[37] and it was recently confirmed by accurate Monte Carlo simulation[38], and $\tau = 23$ fs for InN, which was measured with the ultra-fast photoluminescence technique by Jang et al.[39]. Next, for each ternary, τ was determined with a linear fitting procedure between these two limits. The values of τ and the thermal conductivity κ applied in our equations to obtain the transport parameter and ZT are reported in Table 6 in the Supplementary Information. A dense mesh of up

to 2000 k-points in the first Brillouin zone was used to calculate these parameters. These calculations did not include the effect of spin–orbit coupling, which was shown to be irrelevant for this class of materials[40].

2.2. Computational Models

As mentioned above, the thermodynamically stable structure is wurtzite for both GaN and InN, where this hexagonal structure belongs to the $P6_3mc$ space group, with lattice parameters in $\mathring{A}$ equal to $a = 3.19 and c = 5.18$, and $a = 3.54 and c = 5.70$, respectively[41, 42]. The unit cell has two units for GaN (or InN) with an XN_4 (X = Ga or In) tetrahedron depicted as alternating planes of tetrahedrally coordinated nitrogen and Ga (or In) atoms stacked alternatively along the c-axis.

In order to assess the computational setup, preliminary characterization of the structural and electronic properties of the binaries was performed. The good agreement between the B3LYP-17 results and experimental data is shown in Table 1 in the Supplementary Information [17, 43, 44], where the optimized lattice parameters are also reported.

To design the ternary structures, $In_xGa_{1-x}N$, and analyze the effect of the In content on different properties, a $[2 \times 2 \times 2]$ supercell containing 32 atoms was modeled, as depicted in Fig. 1. The full composition range of $0 < x < 1$ was investigated with minimum/maximum value of $x = 0.0625/0.875$, respectively.

In order to verify the tendency to cluster into Ga/In separated sublattices, two different solid solutions were designed and analyzed, corresponding to the same percentage of In, namely $x = 0.5$. For clarity, the two structures, shown in Fig. 4 in the Supplementary Information, were called *IGIG* and *IIGG* to highlight the different stacking along the z direction of the four xy-sheets containing In (I) and Ga (G) atoms, respectively.

Finally, to provide first estimates of the roles of localized defects on transport coefficients, an isolated Ga vacancy was created in the ternary $In_{0.2}Ga_{0.8}N$ and the corresponding crystal was studied and compared with the perfect crystal.

All ternary alloys were fully optimized at the B3LYP-17 level to calculate their thermodynamic stability with respect to the original compounds, before studying their band structures, IR signals, and transport properties.

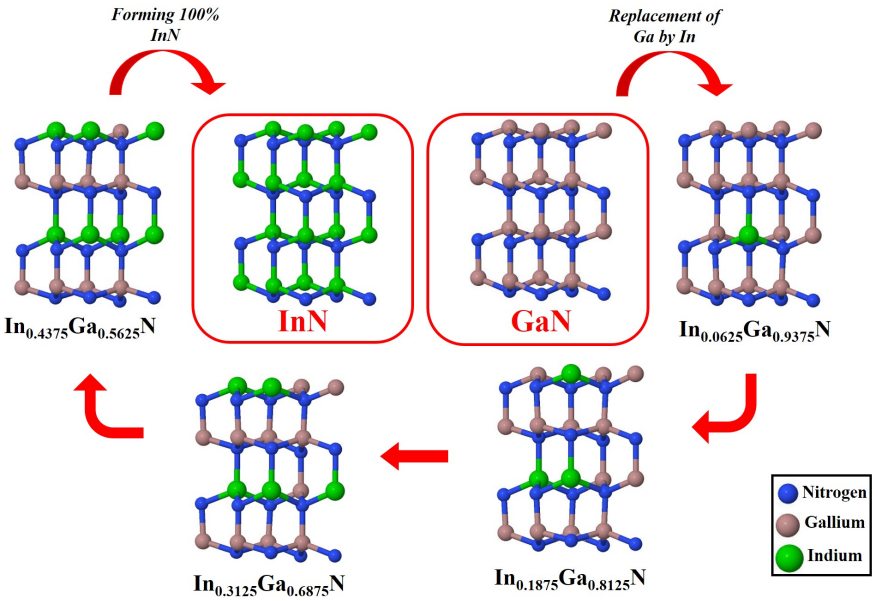

Figure 1: Structures of the [[2 × 2 × 2] supercells for $In_xGa_{1-x}N$ ternary alloys.

3. Results and discussion

3.1. Structural properties

The elemental compositions of ternary $In_xGa_{1-x}N$ compounds have important effects on their physical properties but also on the epitaxial growth process[45]. The variations in the lattice parameters as functions of the In content have been experimentally demonstrated[46, 47] and predicted in several DFT computational studies[44, 17]. Our results are shown in the left panel of Fig. 2.

The deviation from linearity of a given quantity P in a ternary $In_xGa_{1-x}N$ can be estimated using the 2nd order Vegard's law[45] according to the general formula:

$$P(x) = x \cdot P[\mathrm{InN}] + (1-x) \cdot P[\mathrm{GaN}] - b_{\mathbf{P}} \cdot x(1-x), \qquad (1)$$

where the $b_{\mathbf{P}}$ parameter considers the divergence from linearity.
Our results, obtained for the lattice parameters by interpolating the data shown in Fig. 2, indicate a slightly larger deviation for c ($b_{\mathbf{c}} = -0.22 \pm 0.13\,\mathring{A}$) with respect to a ($b_{\mathbf{a}} = -0.0058 \pm 0.0123\,\mathring{A}$) which can probably be ascribed to the relaxation of the In-N bonds along the z-axis.

The results for the bulk modulus, B, and its derivative, B', are shown in Table 1, and they are compared with the experimental values where available. It should be noted that the spread in the observed quantities can be rather large, such as in the case of B, where we found values of 207[48], 190[49] and 175[50] GPa for GaN, and 152[51], 139[48], and 127[49] GPa for InN. The bowing parameter $b_{\mathbf{B}}$ associated with B and calculated according to Eq. 1 ($P \equiv B$) agreed perfectly with the value of 29 GPa obtained by Teles et al.[52] based on highly accurate *ab initio* cluster calculations.

Overall, the structural characterizations of the ternary alloys appeared to be accurate, thereby confirming the reliability of the models and computational setup.

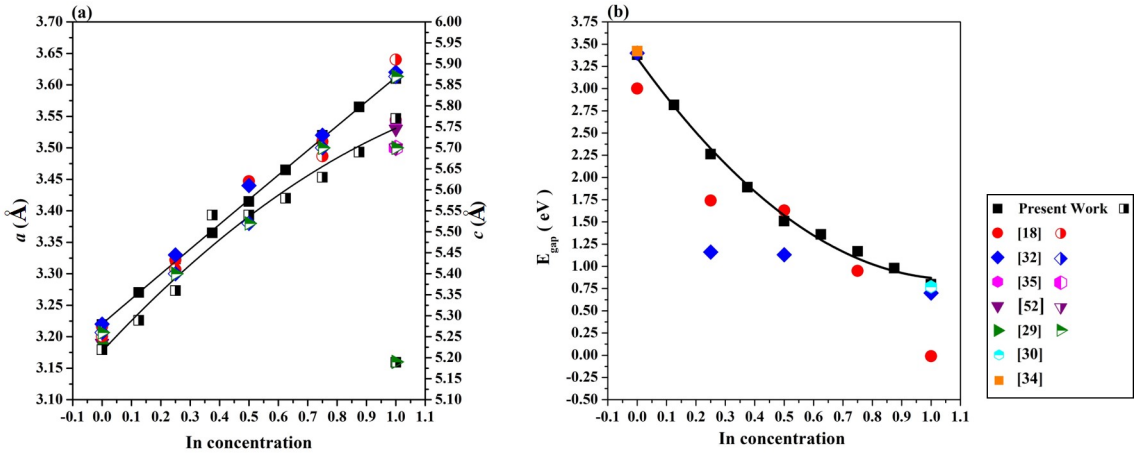

Figure 2: Lattice parameters **a** and **c** (left panel), and energy band gap E_{gap} (right panel) as functions of the In concentration ($0 < x < 1$) in the ternaries $\text{In}_x\text{Ga}_{1-x}\text{N}$.

3.2. Electronic properties

The application of these semiconductors in optoelectronics depends greatly on their electron band gap and band structure. Thus, accurate estimates of these properties are fundamentally important for determining the main characteristics of the materials. In particular, at the B3LYP-17 level, the direct band gaps of GaN and InN are close to the experimental values, as shown in Table 1.

The band gap values for different alloys as functions of the In contents are shown in the right panel of Fig. 2. Van Schilfgaarde et al.[53] used Vegard's

%In	E_{gap} (eV)		B (GPa)		B'	
		Ref		*Ref*		*Ref*
0 (GaN)	3.39	3.42[a]	197.4	190.3[d]	3.92	4.51[d]
6	3.07		188.2		4.03	
12	2.81		183.6		4.05	
25	2.26	2.46[b]	179.4	158.9[d]	4.07	4.36[d]
30	2.05		175.1		4.10	
37	1.89		171.2		4.11	
43	1.66		166.6		4.11	
50	1.51	1.63[b]	162.5	147.9[d]	4.10	4.38[d]
65	1.36		157.5		4.18	
75	1.17	1.32[b]	152.1	135.9[d]	4.23	4.44[d]
87	0.98		146.7		4.24	
100 (InN)	0.79	0.78[c]	141.4	139.1[f]	4.25	4.52[d]

Table 1: Structural properties of mixed alloys $In_xGa_{1-x}N$ at the B3LYP-17 level. Previously reported results (where available) are presented for comparison in columns *Ref. a: Ref. [46], b: Ref. [17], c: Ref. [47], d: Ref. [49], and f : Ref. [48].*

approach and proposed a parabolic fitting for E_{gap}, as given in Eq. 1. A large value of $b_{\mathbf{gap}}$ indicates a strong influence of the alloys concentration on the energy gap. Our value of $b_{\mathbf{gap}} = 2.12$ eV is close to the value of 3.2 eV determined recently for strained ternary alloys by Kour et al.[54].

In order to understand the influence of the indium content on ternary alloys and to examine the band structure in detail, we compared the projected density of states (PDOS) for the binary compounds with those for the mixtures. In all cases, the main gap was found between crystalline orbitals with a strong *p*-N character (highest occupied crystalline orbitals, *HOCO*) and lowest unoccupied crystalline orbitals, *LUCO*, with relevant In/Ga contributions.

In the case of indium nitride, the significant hybridization between In and N high energy *p* orbitals imparts a strong *p* character to the first unoccupied band that considerably reduces the gap in Γ (right upper panel of Fig. 1 in the Supplementary Information).By contrast, the *HOCO* in GaN has a remarkable contribution from the *s* and *d* orbitals of gallium, thereby resulting in a shift of the *LUCO* toward relatively higher energy values (left upper panel of Fig. 1 in the Supplementary Information).

As expected, the closing of the gap for $In_xGa_{1-x}N$ systems can be ascribed to

the appearance of In-*sp* states in the lower part of the conduction bands. This effect is particularly evident when the In concentration increases, as shown in the bottom panel of Fig. 1 in the Supplementary Information, where the PDOS is presented for the ternary alloy corresponding to $x = 0.875$.

The reduction of the main gap and the indium nature of the states that enter the lower part of the virtual bands are already visible in the alloys with a lower In content, such as $In_{0.2}Ga_{0.8}N$. The latter appears to have good transport properties, which is why its electronic structure is shown in Fig. 3.

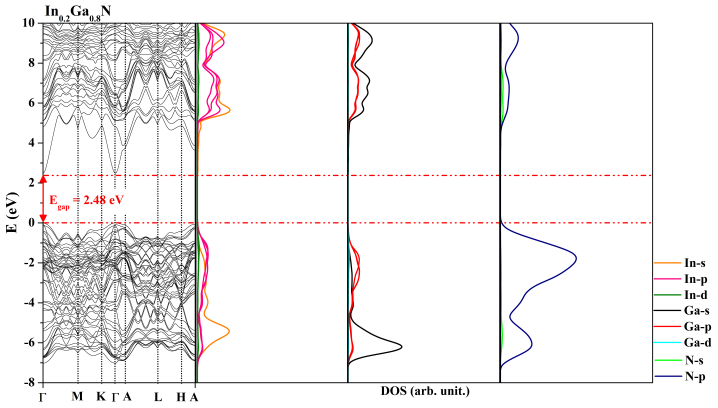

Figure 3: Band structure and PDOS for the ternary alloy $In_{0.2}Ga_{0.8}N$.

3.3. Thermodynamic properties

The thermodynamic properties are essential for obtaining insights into the physical chemistry of alloys and assessing their possible applications in optical devices. In this context, it is particularly important to determine the stability of the ternary mixtures with respect to the binary compounds as a function of the molar fraction, x, and temperature, T.

The significance of determining all of the contributions to the self-consistent free energy was discussed in a previous study [55]. In particular, including the lattice vibrations leads to a large reduction in the order–disorder critical temperature and changes the shape of the solubility and spinodal curve. Thus, we calculated the Gibbs free energy for each compound by considering both the energetic (E_{vib}) and entropic (S_{vib}) thermal contributions on the basis of the vibrational frequencies in Γ:

$$G(T) \;=\; E_{\mathrm{el}} + ZPE + E_{\mathrm{vib}}(T) + PV - TS_{\mathrm{vib}}(T), \qquad (2)$$

where $E_{\rm el}$ is the electron energy and ZPE indicates the zero-point contribution of the vibrational energy. We then estimated the Gibbs formation energy by referring to the following reaction:

$$x\,InN + (1-x)\,GaN \quad \Rightarrow \quad In_xGa_{1-x}N \tag{3}$$

as

$$\Delta G_{\rm form}(T) = G[In_xGa_{1-x}N](T) - x\,G[InN] - (1-x)\,G[GaN] \tag{4}$$

for several temperatures. Finally, within the limit of an ideal binary solution, we added the mixing entropic contribution, which depends only on x:

$$\Delta S_{\rm mix} \;=\; -k_B\,[x\ln x + (1-x)\ln(1-x)], \tag{5}$$

where k_B is the Boltzmann constant, in order to obtain the total Gibbs free energy:

$$\Delta G_{\rm tot}(T) \;=\; \Delta G_{\rm form}(T) - T\Delta S_{\rm mix}. \tag{6}$$

Comparisons of the values for $\Delta G_{\rm tot}$ and $\Delta G_{\rm form}$ at room temperature (as shown in Table 1 in the Supplementary Information) demonstrate the fundamental role of $S_{\rm mix}$ in the stabilization of the ternary alloys.

The general trend in the indium solubility in GaN was reproduced. Indeed, our energy values are within the ranges of previously reported computed data. Our Gibbs free energy at 298 K for $x = 0.5$ is 72 meV/atom and can be compared with mixed enthalpies obtained by Ferhat et al.[56] (34 meV/atom, by performing local-density calculations on periodic models) and by Teles et al.[52] (50 meV/atom at 800 K, by employing a cluster expansion approach).

As previously reported, the large values of $\Delta G_{\rm form}$ suggest high critical temperatures and a tendency for immiscibility in a wide composition range. Studying $\Delta G_{\rm tot}$ as a function of x allowed us to calculate the phase diagrams for $In_xGa_{1-x}N$. As already suggested[52, 56], the mismatch in the lattice parameters for the binary InN and GaN leads to an extended miscibility gap accompanied by spinodal decomposition, as shown in Fig. 5. Finally, our estimate critical temperature of 1600 K is in good agreement with the DFT value of 1654 K calculated by Gan et al.[55].

Regarding the *IGIG* and *IIGG* structures ($x = 0.5$), although their structural and electronic properties are extremely similar (as shown in Table 3 in the Supplementary Information), *IGIG* is ≈ 5 meV/atom more stable than *IIGG* at room temperature. More realistic models would be beneficial but on the basis of this first rough analysis it is possible to affirm that the formation of stacked Ga/In interfaces is a more expensive process with respect to a homogeneous solution between the two atoms.

Finally, we estimated that the formation of the Ga vacancy in the ternary $In_{0.2}Ga_{0.8}N$ is 0.08 eV/atom more expensive than that in the binary GaN compound.

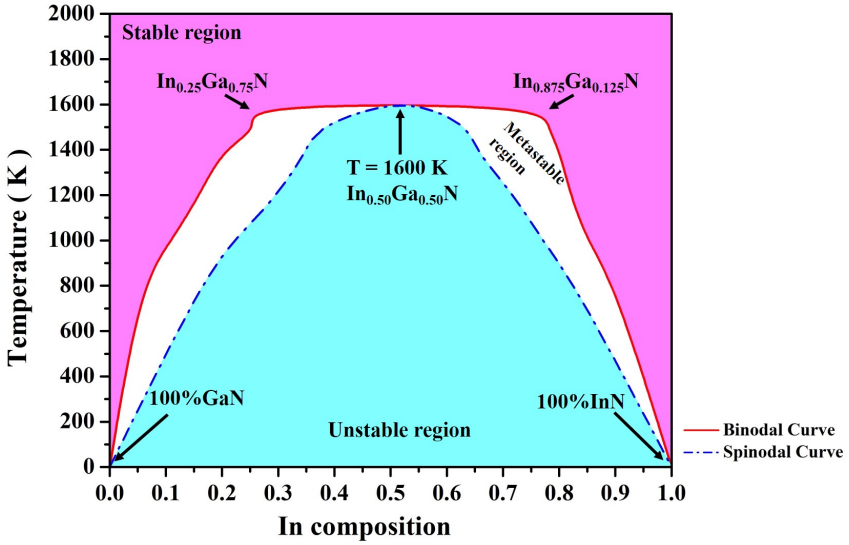

Figure 4: Spinodal and binodal curves obtained for GaN/InN ternary alloys.

3.4. Transport properties

III-Nitrides are promising candidates for use in highly efficient thermoelectric materials and devices because of their unique characteristics. In fact, in order to operate in a high temperature regime, a material must exhibit both temperature stability and a wide band gap ($> 10k_bT$) to prevent the excitation of minority carriers. $In_xGa_{1-x}N$ alloys satisfy both of these criteria and our computational approach accurately reproduced aspects related

to their geometric and electronic structures. Thus, we can complete the characterization of these ternaries by describing their transport features.

To guide our analysis, we provide a summary of the major previously reported experimental observations.

The effects of the carrier density, c_d, indium composition, and temperature on the thermoelectric performance of $In_xGa_{1-x}N$ alloys were investigated by several experimental groups[57, 58, 14, 59]. Despite the various synthetic paths employed, there is considerable agreement regarding some key issues. In particular, (i) the majority of the samples had negative Seebeck coefficient values, thereby suggesting n-type behavior, and (ii) the main thermoelectric parameters, i.e., S, σ, and power factor, increased as the temperature increased.

The dependency of the thermoelectric properties on the indium concentration is more difficult to investigate because several effects can occur simultaneously and they sometimes act in opposite directions.

The thermal conductivity $\kappa = \kappa_p + \kappa_e$ decreases as the percentage of indium increases. The phonon contribution value, κ_p, decreases by over one order of magnitude when the indium content changes from zero to 19%[57] due to two processes that tend to reduce the mean free path of phonon dispersion through the lattice, i.e., increased strain and the step up of defects. Despite the reduced mobility caused by the lower electron effective mass of InN (0.11 m_e) compared with that of GaN (0.20 m_e), the electrical conductivity, σ, increases with the indium composition due to the enhanced carrier density, which dominates the electron transport mechanism. High values of the Seebeck coefficient, S, of $\approx$ -500 μV K^{-1} corresponding to a power factor of around $24 \cdot 10^{-4}$ W $m^{-1}K^{-2}$, were observed in alloys with $x_{In} \approx 0.1$ in several studies[59, 43]. However, as the doping increased, both S and PF gradually decreased because of the different effects outlined above.

In summary, for $5\% < x_{In} < 30\%$, (i) κ and PF decrease whereas (ii) σ and ZT increase, and (iii) all of the properties increase with the temperature, thereby confirming the possibility of using $In_xGa_{1-x}N$ alloys in high temperature thermoelectric applications.

Nevertheless, the optimal value for In doping in this range is still controversial. At room temperature, Nakamura et al.[57] determined an optimal carrier concentration of $1.1 \cdot 10^{19}cm^3$ and obtained $ZT = 0.04$ for a sample containing 17% indium. Kucukgok et al.[59] obtained a figure of merit of 0.072 for a sample with 20% In and at the same temperature, Pantha et al.[14] obtained a ZT value of 0.08 for an alloy with 36% In and a carrier

concentration around $1 \cdot 10^{20}$ cm^{-3}.

As expected, the path employed to synthesize a sample and its unique characteristics have fundamental effects on the thermoelectric features of each material, thereby making theoretical modeling highly complicated. Moreover, our computations require two parameters, τ and κ, which can be obtained from experiments. Therefore, to perform our analysis, we focused on the homogeneous and complete data set presented by Kucukgok et al.[59] for $In_xGa_{1-x}N$ alloys in the range 0< In< 25%. For each compound, we calculated the values of S, σ, and PF at the experimental value of the carrier density, c_d, and used the experimental thermal conductivities to estimate the figure of merit. Despite the poor quantitative agreement (Table 6 in the Supplementary Information provides point-to-point comparisons), our calculations reproduce all of the main thermoelectric characteristics of the experimental samples.

In particular, in the composition range explored: (i) we obtained negative Seebeck coefficients, and thus a preference for the n-type conduction; (ii) as shown in Fig. 5, S and PF decreased as the indium percentage increased, whereas the electrical conductivity stepped up; (iii) in good agreement with the experimental evidence presented by Kucukgok et al. and other studies[43, 57], all of these quantities increased with the temperature (as shown in Fig. 2 in the Supplementary Information); and (iv) ZT reached a maximum value for $x = 0.2$, although this is lower than the experimental result (0.026 *vs* 0.072 at room temperature, it increases till 0.2 at 900 K). Hence, based on our calculations, the $In_{0.2}Ga_{0.8}N$ alloy appears to be the best candidate for thermoelectric applications.

We then tried to understand the dependence of the transport parameters on the carrier density. As described by Sztein et al.[19], we calculated S, σ, and ZT at different temperatures for the alloy $In_{0.1}Ga_{0.9}N$ by varying c_d from $1.0\,10^{17}$ to $1.0\,10^{20}$ cm^{-3}. The results shown in Fig. 6 demonstrate that for all temperatures, the Seebeck coefficient decreases monotonously in this interval and the figure of merit reaches a maximum around $c_d = 1.0 \cdot 10^{19}$ cm^{-3}.

Finally, we obtained first estimates of the effects of the incidence of defects on the thermoelectric efficiency by calculating the transport coefficients in the defective alloy $In_{0.2}Ga_{0.8}N$. Despite the higher values of S and σ ($\approx$ -300 *vs* -134 μV K^{-1} and 1629 *vs* 227 Ω^{-1} cm^{-1}), the power factor is lower and ZT has a value of 0.009 at 300 K compared with 0.026 for the perfect ternary.

In summary, despite the strong approximations made by the methods employed, it is possible to predict the trends and general characteristics of

$In_xGa_{1-x}N$ compounds, and modeling defects (interstitial, doping, structural, etc.) may facilitate the engineering of promising materials.

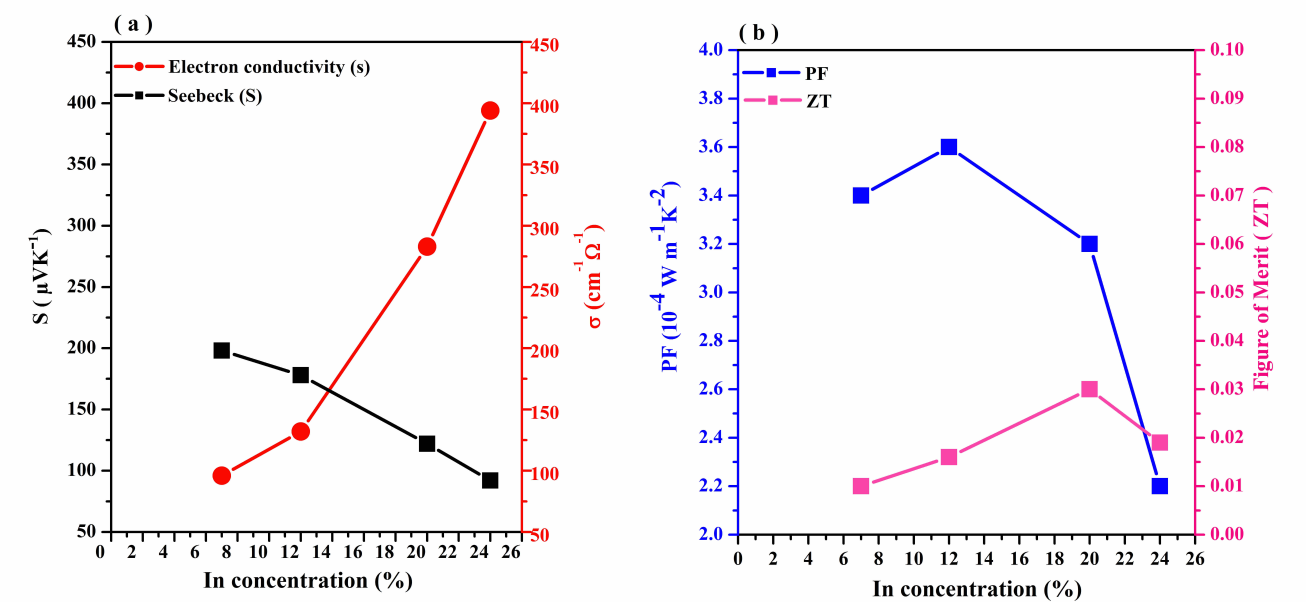

Figure 5: Absolute values of the Seebeck coefficient S and σ (a), and PF and ZT (b) as functions of the In content in the range of $0 < x < 0.24$ evaluated at the B3LYP-17 level. The corresponding density carrier and τ and κ values are listed in Table 6 in the Supplementary Information.

3.5. Vibrational Properties

IR spectroscopy was used to elucidate the structures of the different alloys on the atomic scale. We computed the spectra in order to show the possibility of assessing the composition of the supercell in terms of the In percentage and revealing the presence of any defects in the crystal. We describe both of these features in the following.

To allow comparisons, the spectral fingerprints of the two binary alloys are presented in Fig. 5 in the Supplementary Information. The two clear peaks correspond to the A and E symmetry modes of the N-Ga/In bonds. Interestingly, the formation of the ternary compounds leads to splitting of the signals because of the interactions between nitrogen with Ga and In. According to the spectra shown in Fig. 5 in the Supplementary Information,

the presence of small quantities of indium within the GaN matrix can be unambiguous detected and some conclusions on the amount of doping can be derived. In the case of $In_{0.065}Ga_{0.935}N$ (light blue line), the two characteristic peaks for GaN are shifted toward lower frequencies and a small shoulder appears around 570 cm^{-1}, and as the percentage of In increases (violet line), one of the characteristic InN modes emerges ($\approx$ 450 cm^{-1}) and the shoulder merges with the signal for GaN.

The IR spectra for *IGIG* and *IIGG* alloys are compared in the right panel of Fig. 7. The two alloys are almost indistinguishable based on the volume, lattice, and elastic parameters, but their spectral features differ due to the appearance of two distinct signals at 473 and 551 cm^{-1}, which allow the assignment of the green signal to the *IIGG* system.

Finally, in the left panel of Fig. 7, the IR spectrum for the alloy $In_{0.2}Ga_{0.8}N$ where a Ga vacancy is created is compared with that of the corresponding perfect ternary, which shows that new broad peaks emerge below 400 cm^{-1} and in the region between 600–750 cm^{-1}, due to the vibrational modes of the under-coordinated nitrogen atoms.

4. Conclusions

By designing a 32-atom supercell and conducting analyses at the B3LYP-17 level, we determined the effects of In doping on the structural parameters, band gap, thermodynamic stability, transport properties, and IR fingerprints of the $In_xGa_{1-x}N$ ternary alloys in the entire composition range. Preliminary studies of the role of defects were also conducted.

We accurately calculated the main structural parameters (volume and lattice bowing parameters) and electronic characteristics (band gap and density of states) for these compounds, and our results are in good agreement with previously reported experimental and theoretical data. The computed frequencies and IR spectra provide clear insights into the structures of these materials on an atomic scale.

The thermodynamic range of stability was reproduced well for the ternaries. In particular, the doping of GaN alloy with In occurs almost spontaneously at temperatures up to 500 K, and thermodynamically stable alloys are produced with improved thermoelectric performance and promising applications. We confirmed that $In_xGa_{1-x}N$ are n-type conductors and that good performance can be achieved with about 20% In doping.

In this study, we obtained reliable characterizations of $In_xGa_{1-x}N$ ternary alloys to facilitate further more realistic investigations, i.e., defective models.

5. Acknowledgments

This study was supported by the Algerian Government through a grant provided by the *Exceptional National Program* PNE in collaboration with the Algerian Ministry of Higher Education and Scientific Research.
The Fundação de Amparo à Pesquisa do Estado de São Paulo (FAPESP) (grant n. 2016/25500-4, 2019/12430-6) is also greatly acknowledged.
The authors are extremely grateful to the CINECA Supercomputing Center, which supported this study by providing computational resources through the ISCRA Class C Project, code HP10CP7ETO.

References

[1] C. Zhou, A. Ghods, V. G. Saravade, P. V. Patel, K. L. Yunghans, C. Ferguson, Y. Feng, B. Kucukgok, N. Lu, I. T. Ferguson, Review: Current and emerging applications of the III-Nitrides, J. Solid State Sci. Technol. 6 (2017) Q149–Q156.

[2] A. Hangleiter, III-IV Nitrides: A new age for optoelectronics, MRS Bulletin 28 (2003) 350–353.

[3] A. Kafi, F. D. Khodja, F. Saadaoui, S. Chibani, A. Bentayeb, M. D. Khodja, An ab initio study of the structural and optoelectronic properties of $Al_xGa_{1-x}N$ (x = 0, 0.125, 0.375, 0.625, 0.875 and 1) semiconductors., J. Comput. Electron. 19 (2020) 26–37.

[4] B. Amin, I. Ahmad, M. Maqbool, S. Goumri-Said, R. A. R, Ab initio study of the bandgap engineering of $Al_{1-x}Ga_xN$ for optoelectronic applications, J Appl Phys. 109 (2011) 023109.

[5] M. A. der Maur, A. Pecchia, G. Penazzi, W. Rodrigues, A. D. Carlo, Efficiency drop in green InGaN/GaN light emitting diodes: The role of random alloy fluctuations, Phys. Rev. Lett. 116 (2016) 027401.

[6] F. A. Ponce, D. P. Bour, Nitride-based semiconductors for blue and green light-emitting devices., Nature 386 (1997) 351359.

[7] T. Mukai, M. Yamada, S. Nakamura, Characteristics of InGaN-based UV/blue/green/amber/red light-emitting diodes, Jpn. J. Appl. Phys. 38 (1999) 3976–3981.

[8] Y. Li, Y. Jiang, J. Die, C. Wang, S. Yan, Z. Ma, H. Wu, L. Wang, H. Jia, W. Wang, H. Chen, Improvement of green InGaN-based LEDs efficiency using a novel quantum well structure, Chinese Physics B 26 (2017) 087311.

[9] R. Kour, S. Arya, S. Verma, A. Singh, P. Mahajan, A. Khosla, Review: Recent advances and challenges in indium gallium nitride $In_xGa_{1-x}N$ materials for solid state lighting, J. Solid State Sci. Technol. 9 (2019) 015011.

[10] J. W. A. III, W. Walukiewicz, High efficiency, radiation-hard solar cells, LBNL Report 56326 (2004) 1–18.

[11] B. N. Pantha, A. Sedhain, J. Li, J. Y. Lin, H. X. Jiang, Electrical and optical properties of p-type InGaN, Applied Physics Letters 95 (2009) 261904.

[12] R. Singh, D. Doppalapudi, T. D. Moustakas, L. T. Romano, Phase separation in InGaN thick films and formation of InGaN/GaN double heterostructures in the entire alloy composition, Applied Physics Letters 70 (1997) 1089–1091.

[13] X. Ruan, F. Zhang, W. Zhang, First-principles study on electronic structure and optical properties of In-doped GaN, J. Theor. Comput. Chem. 13 (2014) 1450070.

[14] B. N. Pantha, R. Dahal, J. Li, J. Y. Lin, H. X. Jiang, G. Pomrenke, Thermoelectric properties of $In_xGa_{1x}N$ alloys., Appl Phys Lett. 28 (2008) 042112.

[15] A. D. Vito, A. Pecchia, A. D. Carlo, M. A. der Maur, Characterization of non-uniform InGaN alloys: spatial localization of carriers and optical properties., Jpn. J. Appl Phys. 58 (2019) SCCC03.

[16] H. Qin, X. Luan, C. Feng, D. Yang, G. Zhang, Mechanical, thermodynamic and electronic properties of Wurtzite and Zinc-Blende GaN crystals., Materials 12 (2017) 1419.

[17] M. Shakil, M. K. Masood, M. Zafar, S. Ahmad, A. Hussain, M. A. Gadhi, Theoretical study of structural, electronic and optical properties of $In_xGa_{1-x}N$ alloys., Optik 174 (2018) 739 47.

[18] M. Zafar, M. K. Masood, M. Rizwan, A. Zia, S. A. S, A. Akram, C. C. Bao, M. Shakil, Theoretical study of structural, electronic, optical and elastic properties of $Al_xGa_{1-x}P$., Optik 182 (2019) 1176 85.

[19] A. Sztein, J. Haberstroh, J. E. Bowers, S. P. DenBaars, S. Nakamura, Calculated thermoelectric properties of $In_xGa_{1-x}N$, $In_xAl_{1-x}N$ and $Al_xGa_{1-x}N$, J. of Applied Physics 113 (2013) 183707.

[20] A. D. Becke, Density-functional thermochemistry. III The role of exactexchange, J. Chem. Phys. 98 (1993) 5648.

[21] S. H. Vosko, L. Wilk, M. Nusair, Accurate spin-dependent electronliquid correlation energies for local spin density calculations: a critical analysis, Can. J. Phys. 58 (1980) 1200.

[22] R. Dovesi, A. Erba, R. Orlando, C. Zicovich-Wilson, B. Civalleri, L. Maschio, M. Rérat, S. Casassa, J. Baima, S. Salustro, B. Kirtman, Quantum-mechanical condensed matter simulations with crystal, WIRES. Mol. Sci. 8 (4) (2018) e1360.

[23] F. Corà, M. Alfredsson, G. Mallia, D. Middlemiss, W. Mackrodt, R. Dovesi, R. Orlando, In Principles and Applications of Density Functional Theory in Inorganic Chemistry II, Springer, Heidelberg, 2004.

[24] R. Pandey, J. Jaffe, N. Harrison, Ab-initio study of high-pressure phase-transition in GaN, Journal of Physics and Chemistry of Solids 55 (1994) 1357–1361.

[25] J. Rothballer, F. Bachhuber, S. M. Rommel, T. Söhnel, R. Weihrich, Origin and effect of In-Sn ordering in $InSnCo_3S_2$: a neutron diffraction and DFT study, RSC Adv. 4 (2014) 42183–42189.

[26] R. Dovesi, M. Causà, R. Orlando, C. Roetti, Ab initio approach to molecular crystals: a periodic hartree-fock study of crystalline urea, J. Chem. Phys. 92 (1990) 7402–7411.

[27] N. L. Marana, G. B. Pinhal, J. A. S. Laranjeira, P. G. C. Buzolin, E. Longo, J. R. Sambrano, Strain-induced novel properties of alloy nitride nanotubes., Comput Mater Sci. 177 (2020) 109589.

[28] G. P. GB, M. NL, F. GSL, S. JR., Structural, electronic and mechanical properties of single-walled AlN and GaN nanotubes via DFT/B3LYP, Theor Chem Acc. 138 (2019) 31.

[29] R. Dovesi, V. R. Saunders, C. Roetti, R. Orlando, C. M. Zicovich-Wilson, F. Pascale, B. Civalleri, K. Doll, N. M. Harrison, I. J. Bush, P. D'Arco, M. Llunell, M. Causà, Y. Noël, L. Maschio, A. Erba, M. Rerat, S. Casassa, CRYSTAL17 User's Manual, Università di Torino, Torino (2017).

[30] D. Shanno, Conditioning of quasi-newton methods for function minimization, Math. Comput. (1970) 647.

[31] C. Zicovich-Wilson, R. Dovesi, On the use of symmetry adapted crystalline orbitals in SCF-LCAO periodic calculations. I. the construction of the symmetrized orbitals, Int. J. Quantum Chem. 67 (1998) 299.

[32] F. D. Murnaghan, The compressibility of media under extreme pressures, Proc. Natl. Acad. Sci. U.S.A. 30 (1944) 244.

[33] A. Erba, A. Mahmoud, D. Belmonte, R. Dovesi, High pressure elastic properties of minerals from ab initio simulations: The case of pyrope, grossular and andradite silicate garnets, J. Chem. Phys. 140 (12) (2014) 124703.

[34] C. Zicovich-Wilson, F. J. Torres, F. Pascale, L. Valenzando, R. Orlando, R. Dovesi, Ab initio simulation of the ir spectra of pyrope, grossular and andradite, J. Comput. Chem. 29 (2008) 2268–2278.

[35] M. Lundstrom, Fundamentals of Carrier Transport, Cambridge University Press, UK, 2009.

[36] G. Sansone, A. Ferretti, L. Maschio, Ab initio electronic transport and thermoelectric properties of solids from full and range-separated hybrid functionals, J. Chem. Phys. 147 (11) (2017) 114101.

[37] N. M. Stanton, A. J. Kent, A. V. Akimov, P. Hawker, T. S. Cheng, C. T. Foxon, Energy relaxation by hot electrons in N-GaN epilayers, J. Appl. Phys. 89 (2001) 973.

[38] S. Wang, Y. Dou, H. Liu, Z. Lin, H. Zhang, Electron momentum and energy relaxation times in wurtzite GaN, InN and AlN: A monte carlo study, J. Electr. Mat. 47 (2018) 1560–1568.

[39] D. J. Jang, G. T. Lin, C. L. Wu, C. L. Hsia, L. W. Tu, M. E. Lee, Energy relaxation of InN thin film, Appl. Phys. Lett. 91 (2007) 092108.

[40] L. E. Ramos, L. K. Teles, L. M. R. Scolfaro, J. L. P. Castineira, A. L. Rosa, J. R. Leite, Structural, electronic, and effective-mass properties of silicon and zinc-blende group-iii nitride semiconductor compounds, Phys. Rev. B 63 (2001) 165210.

[41] H. Schulz, K. H. Thiemann, Crystal structure refinement of AlN and GaN., Solid State Commun. 23 (1977) 815819.

[42] J. Wu, W. Walukiewicz, K. M. Yu, J. W. A. III, E. E. Haller, H. Lu, W. J. Shaff, Y. Saito, Y. Nanishi, Unusual properties of the fundamental band gap of inn., Appl Phys Lett. 80 (2002) 3967.

[43] S. Surender, S. Pradeep, K. Prabakaran, S. M. Sumithra, S. Singh, K. Baskar, The role of indium composition on thermo-electric properties of InGaN/GaN heterostructures grown by MOCVD, J. of Alloys and Compounds 734 (2018) 48,54.

[44] X. Wang, W. Liu, C. Zhai, J. Yun, Z. Zhang, Dft calculation on the electronic structure and optical properties of $In_xGa_{1-x}N$ alloy semiconductors, Mater Sci. 26 (2019) 127,132. doi:10.5755/j01.ms.26.2.21569.

[45] B. T. Liou, S. H. Yen, Y. K. Kuo, Vegards law deviation in band gap and bowing parameter of $Al_xIn_{1-x}N$, Appl Phys A. 81 (2005) 651,655.

[46] V. Bougrov, M. E. Levinshtein, S. L. Rumyantsev, A. Zubrilov, Properties of Advanced Semiconductors Materials GaN, AlN, InN, BN, SiC, SiGe, Wiley, 2001.

[47] J. Wu, W. W. K. M. Yu, J. W. Ager-III, E. E. Haller, H. Lu, W. J. Schaff, Small band gap bowing in $In_{1-x}Ga_xN$ alloys, Appl Phys Lett. 80 (2002) 4741.

[48] A. F. Wright, J. S. Nelson, Consistent structural properties for AlN, GaN, and InN, Phys Rev B. 51 (1995) 7866.

[49] B. T. Liou, Study of lattice constant and bulk modulus in zincblende ingan using local density approximation and generalized gradient approximation., Jpn J Appl Phys. 47 (2008) 3350 3.

[50] H. Achour, S. Louhibi-Fasla, F. Mana, Theoretical investigation of gan, Physics Procedia 55 (2014) 17–23.

[51] Z. Dridi, B. Bouhafs, P. Ruterana, First-principles investigation of lattice constants and bowing parameters in wurtzite $Al_xGa_{1-x}N$, $In_xGa_{1-x}N$ and $In_xAl_{1-x}N$ alloys., Semicond Sci Technol. 18 (2003) 850.

[52] L. K. Teles, J. Furthmüller, L. M. R. Scolfaro, J. R. Leite, F. Bechstedt, Firt-principles calculations of the thermodynamic and structural properties of strained $In_xGa_{1-x}N$ and $Al_xGa_{1-x}N$ alloys, Phys. Rev. B 62 (2000) 2475.

[53] M. van Schilfgaarde, A. Sher, A. B. Chen, Theory of AlN, GaN, InN and their alloys, J. of Crystal Growth 178 (1997) 8–31.

[54] R. Kour, S. Arya, S. Verma, A. Singh, P. Mahajan, A. Khosla, Recent advances and challenges in indium gallium nitride ($in_xga_{1-x}n$) materials for solid state lighting., J. Solid State Sci Technol. 9 (2020) 015011.

[55] C. K. Gan, Y. P. Feng, D. J. Srolovitz, First-principles calculation of the thermodynamics of $In_xGa_{1x}N$ alloys: Effect of lattice vibrations, Phys. Rev. B 73 (2006) 235214.

[56] M. Ferhat, F. Bechstedt, First-principles calculations of gap bowing in $In_xGa_{1x}N$ and $In_xAl_{1x}N$ alloys: Relation to structural and thermodynamic properties., Phys Rev B. 65 (2002) 075213.

[57] A. Sztein, H. Ohta, J. E. Bowers, S. P. DenBaars, S. Nakamura, High temperature thermoelectric properties of optimized ingan, J. of Applied Physics 110 (2011) 123709.

[58] X. Shi, L. Chen, C. Uher, Recent advances in high-performance bulk thermoelectric materials, Int. Mater. Rev. 61 (6) (2016) 379–415.

[59] B. Kucukgok, X. Wu, X. Wang, Z. Liu, I. T. Ferguson, N. Lu, The structural properties of InGaN alloys and the interdependence on the thermoelectric behavior, AIP Adv. 6 (2016) 025305.

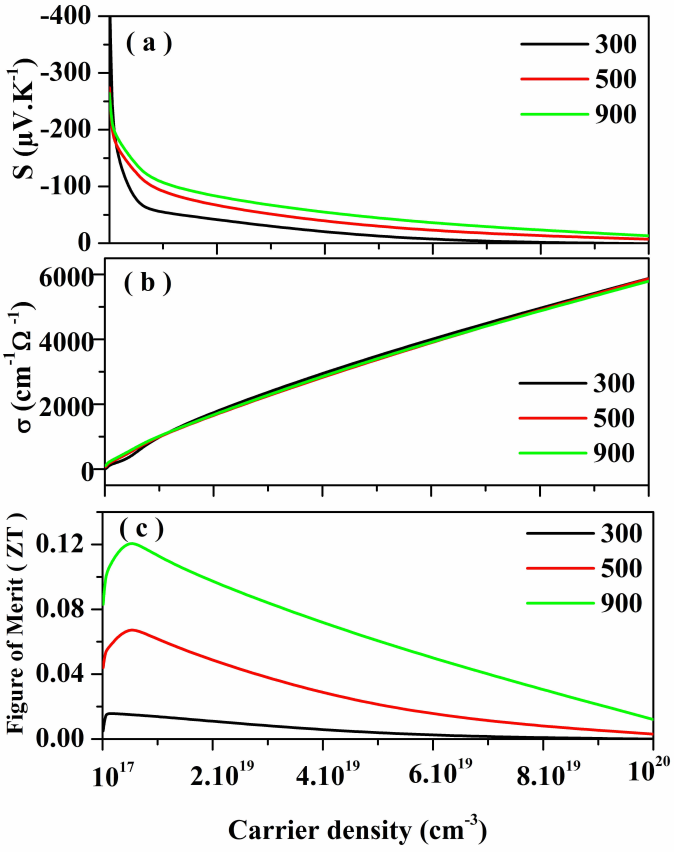

Figure 6: (a) Seebeck coefficient, (b) electrical conductivity, and (c) ZT modeled at various temperatures versus the carrier density for $In_{0.1}Ga_{0.9}N$.

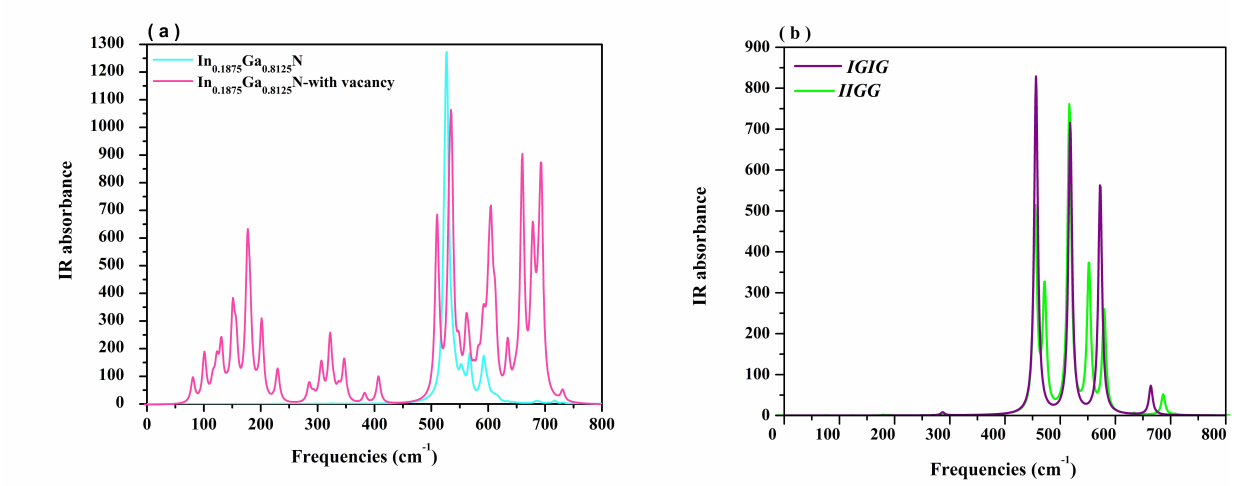

Figure 7: IR spectra in Γ. (a) $In_{0.2}Ga_{0.8}N$ alloy: perfect system (light blue) and system with a Ga vacancy (red). (b) Comparison of the two alloys with 50% In: *IGIG* (violet) and *IIGG* (green).